Anomalous Small-Angle X-ray Scattering Study on the Nanostructure of Co-Sputtered Platinum/Carbon Layers

T. Vad,*,† F. Hajbolouri,‡ H.-G. Haubold,† G. G. Scherer,‡ and A. Wokaun‡,§

Institut für Festkörperforschung, Forschungszentrum Jülich, D-52425 Jülich, Germany, Electrochemistry Laboratory, Paul Scherrer Institut, CH-5232 Villigen, Switzerland, and Laboratorium für Technische Chemie, ETH Zürich, CH-8093 Zürich, Switzerland

Received: March 24, 2004; In Final Form: June 6, 2004

The nanostructures of co-sputtered Pt/C layers were investigated by anomalous small-angle X-ray scattering (ASAXS) experiments with synchrotron radiation. The ASAXS method permits us to separate the platinum-scattering contribution from the carbon background and thus opens up the possibility to retrieve nanostructures formed by the Pt atoms. To obtain the structural information from the scattering data, a columnar structure model is proposed and applied to three different samples prepared with different platinum sputter targets. The results are compared to those obtained from cyclic voltammetry.

Introduction

Commercial electrocatalysts in polymer electrolyte fuel cells (PEFCs) are usually prepared by wet chemical impregnation methods. This preparation consists normally of several deposition, drying, and reduction stages. The catalyst layer is a porous 3-dimensional carbon network on top of which the metal particles, such as Pt or Pt/Ru, are dispersed. During the past decades, a lot of effort has been focused on the development of the polymer electrolyte, electrocatalyst, and electrode materials for PEFCs. The amount of noble metal loading in these electrodes has been dramatically reduced achieving a value around 0.4−0.6 mg metal per cm^2 geometric electrode area. These catalyst loadings are however still too high for making the fuel cell technology cost efficient and competitive to traditional combustion engines. Furthermore, the environmental aspects and the limitation of the noble metal sources are other important reasons for reducing the metal loading of these electrodes. To maintain the electrode performance, especially if the catalyst loading is reduced, the catalyst utilization must be significantly enhanced. Here, utilization is defined as the number of active sites that are accessible to the reactants divided by the total number of catalyst sites in the electrode. The electrode characteristics that control this parameter are the catalyst dispersion, the pore structure in the active layer, and the availability of the three-phase zone, i.e., where the electrochemically active sites, the proton conductive phase, and the reactant gases are all in contact with each other. In very narrow pores, the catalyst particles are encapsulated and the reactant gases do not access the active sites. Hence the development of an alternative electrode preparation technique, where all requirements mentioned above can be fulfilled, is very attractive.

Recently, the sputtering technique has been explored by several research groups in order to reduce the cell costs by manufacturing electrodes with low catalyst loading, where the active layer is localized near the front surface of the electrodes.[2] The sputtering technique, an already well-established and widely used method in the semiconductor industry, is flexible, simple, and allows for the coating of large areas with uniform composition and high reproducibility.[3−5] Furthermore, precious metal recovery and recycling techniques are routinely implemented in high-volume commercial sputter deposition processes. The sputter process is also compatible with other integrated circuit (IC) fabrication technologies, making it ideal for microfuel cell applications.[6]

The idea of sputtering thin films of electrocatalysts on gas-diffusion electrodes (GDE) or directly on membranes (e.g., direct sputtering of Pt onto the surface of Nafion 117 membranes) has been already examined,[2,6,7] but no study has yet been reported where Pt and C were co-sputtered. While a continuously deposited Pt film suffers from the low active surface, it is expected that, by co-sputtering of Pt and C, the active surface can be significantly increased.[8]

For a first test, thin layers of Pt/C were deposited by DC magnetron sputtering on 30 μm Al foil for X-ray experiments and on glassy carbon (GC) substrates for electrochemical measurements.[9] Three samples, prepared with different sputter targets (4 Pt pellets for sample Pt/C(4p), 8 wires for Pt/C(8w), and 4 wires for sample Pt/C(4w)), were investigated. Cyclic voltammetry measurements showed that the Pt/C layers are electrochemically active. Information about the structure and the size of the particles could, however, not be obtained in a first investigation performed on the sample with the lowest Pt loading (4w) by high-resolution scanning electron microscopy (SEM) and transmission electron microscopy (TEM). Therefore, the technique of anomalous small-angle X-ray scattering (ASAXS) [10,11] was applied, which allows us to separate the platinum-scattering contributions from the carbon background, and probes in addition a much larger sample volume than can be achieved by microscopy methods.

Experimental Section

Sample Preparation. Thin layers of Pt/C were deposited on GC (diameter = 1 cm) and Al foil (thickness = 30 μm, 99.999% purity) in a DC-magnetron apparatus built in-house at Paul Scherrer Institut. A graphite target (purity = >99.99%) with

* To whom correspondence may be addressed. Tel.: +49 2461 613593. Fax:+49-2461 612610. E-mail: th.vad@fz-juelich.de.
† Institut für Festkörperforschung.
‡ Paul Scherrer Institut.
§ Laboratorium für Technische Chemie.

10.1021/jp048682q CCC: $27.50
Published on Web 07/27/2004

TABLE 1: Sputtering Conditions for the Three Pt/C Samples

target	Pt/C
base pressure (mbar)	3×10^{-5}
sputter gas	Ar
sputter pressure (mbar)	$1.5-1.6 \times 10^{-2}$
distance target−substrate (cm)	7
sputter power (W)	100

attached Pt wires (diameter = 2 mm) inside the target was used for the co-sputtering of Pt/C (the samples are called Pt/C (4w) and Pt/C (8w), respectively). One graphite target with four pasted Pt pellets (diameter = 4.7 mm) on its top was used for the co-sputtering of the sample with the highest Pt-loading (Pt/C (4p)). The sputtering conditions are given in Table 1.

X-ray Absorption Spectroscopy (XAS). The main reason for performing X-ray absorption measurements for each sample prior to ASAXS studies is to locate each individual Pt-absorption edge that may be shifted by some eVs due to a different chemical bonding. This knowledge is essential for a quantitative evaluation of the contrast variation experiment. The XAS spectra for the three Pt/C samples were recorded in an energy interval of $11.0 \le E \le 12.8$ keV around the Pt L_3 absorption edge for free Pt atoms ($E_{L_3} = 11.564$ keV) at the JUSIFA beamline at DESY-HASYLAB. [12] These spectra contain information on the Pt content in the sample and the valence state of the Pt atoms. From the measured edge jump in the absorption spectrum (see Figure 1)

$$\Delta\mu d = \mu d(E_+) - \mu d(E_-) \tag{1}$$

where μ is the linear absorption coefficient and d is the sample thickness, and the theoretical edge jump for free Pt atoms

$$\Delta\frac{\mu}{\rho} = \frac{\mu}{\rho}(E_+) - \frac{\mu}{\rho}(E_-) \tag{2}$$

where ρ is the material density, and μ/ρ is the mass-absorption coefficient, one obtains the Pt loading m(Pt) of the sample[13,14]

$$m(\mathrm{Pt}) = \frac{\Delta\mu d}{\Delta(\mu/\rho)} \tag{3}$$

E_- denotes the energy immediately before the absorption edge, E_+ the energy immediately after the absorption edge, and $\Delta(\mu/\rho)_{\mathrm{Pt}} = 118.04$ cm^2/g.

From the values $\mu d(E_+)$ and $\mu d(E_-)$, one obtains the normalized absorption spectrum

$$\mu d(E)_{\mathrm{norm}} = \frac{\mu d(E) - \mu d(E_-)}{\mu d(E_+) - \mu d(E_-)} \tag{4}$$

This allows us to directly compare the absorption spectra of samples with different Pt content. From the height of the white line (HWL), [15,16,17] one obtains additional information on the valence state of the Pt atoms by comparison with a reference sample, e.g., a (metallic) Pt foil.

ASAXS Experiments. Contrast variation experiments near the Pt L_3 absorption edge ($E_{L_3} = 11.564$ keV) at energies $E_1 = 11.437$ keV and $E_2 = 11.550$ keV were carried out for all three samples at the JUSIFA beamline. The Pt L_3 absorption edge was chosen because it is easily accessible with the monochromator setup of the beamline (Si-311 double monochromator with an accessible energy range of $5 \le E \le 35$ keV) and because the absorption-edge energy is close to the photon flux maximum ($E_{\max} \approx 12.4$ keV for bending magnets) of the DORIS-III storage ring, thus providing optimal experimental conditions. The concept of contrast variation exploits the fact that the scattering contributions from the Pt structures become energy dependent in the pre-edge region of the L_3 absorption edge (see Figure 7), whereas background scattering contributions such as those from the porous carbon remain unaffected and can be subtracted out (for a more detailed description of a contrast variation experiment, see, e.g., Vad et al.).[14] The resulting ASAXS difference-scattering cross sections $I(E_1) - I(E_2)$ thus reflect the separated scattering from the Pt structures unambiguously.

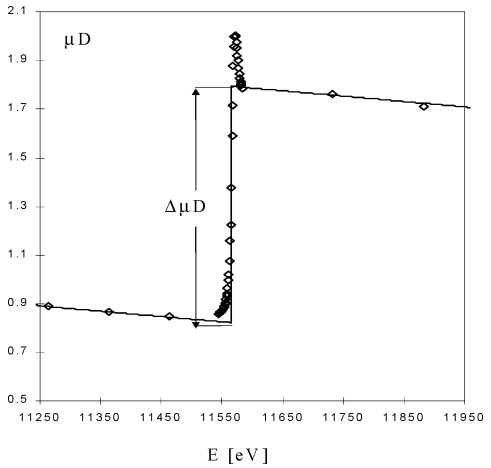

Figure 1. Example for the definition of $\Delta\mu d$. Edge jump of a Pt colloid at the Pt L_3 absorption edge. The solid line is the result from a least-squares fit of pre-edge and postedge data of the X-ray absorption spectrum.[14]

The SAXS intensities at energies E_1 and E_2 and the difference scattering curves $I(E_1) - I(E_2)$, which correspond to the separated scattering contributions of the Pt-structures, are shown in Figure 2.

The shapes of the difference scattering curves of all samples indicate that the platinum does not form a dispersed system of (spherical) particles. All scattering curves exhibit an interparticle correlation peak at Q values around $Q_{\mathrm{peak}} \approx 0.2-0.3$ Å^{-1}. Since the correlation peaks are also present in the separated Pt-scattering curves, the peaks can be related to characteristic distances $D \approx 2\pi/Q_{\mathrm{peak}}$ between Pt particles. A first attempt to model the Pt curves with a locally dense packed system of hard spheres according to Vrij[18] and an additional power law describing the large-scale scattering behavior of these Pt-particle systems led to unphysical results.

Another striking feature, common to all three samples, is a Q^{-2} powerlaw in the low Q range. This powerlaw is characteristic, e.g., for chainlike or columnar (platinum) structures. Therefore, the more plausible model is the one for a columnar structure, since this type of structure is in agreement with the so-called zone model after Movchan, Demchishin (1969), and Thornton (1974)[19,20] (see Figure 3).

The zone model describes the morphology of sputtered layers in dependence of the sputter gas pressure and the substrate temperature. At low substrate temperatures (zone 1), the sputtered film exhibits a pronounced columnar structure with porous regions between the columns. At increased temperatures (zone 2), the structure consists of columns of dense-packed material which are separated by grain boundaries. At very high substrate temperatures (zone 3), the material is almost completely recrystallized and separated by just a few grain boundaries. It seems therefore to be reasonable to model the structure by assemblies of alternating columns of higher and lower

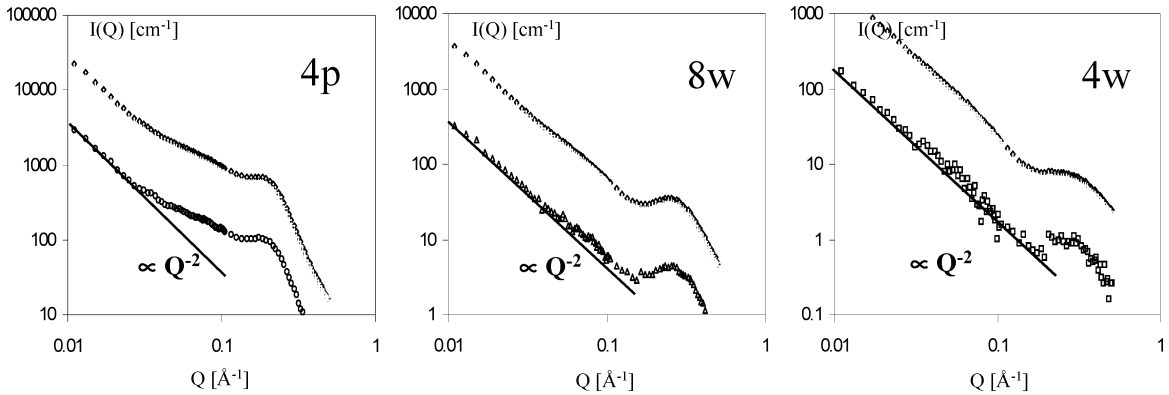

Figure 2. SAXS intensities at energies $E_1 = 11.437$ keV (◇), $E_2 = 11.550$ keV (+), and separated Pt-scattering contributions $I(Q,E_1) - I(Q,E_2)$ for the three Pt/C samples 4p (left), 8w (center), and 4w (right). The low-angle part of all difference scattering curves is proportional to a Q^{-2} power law (inserted solid lines) which indicates chain or columnar Pt structures.

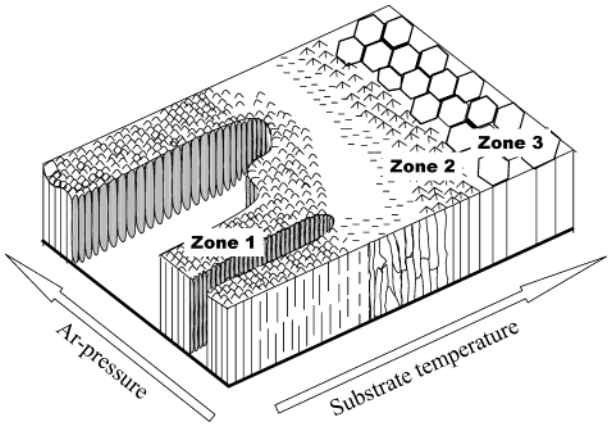

Figure 3. Zone model after Movchan, Demchishin, and Thornton describing the dependence of the layer morphology on substrate temperature and sputter gas pressure.

electron density, whereby all platinum is assumed to reside in the columns of high electron density (see Figure 4).

This assumption is supported by a comparison of the scattering behavior of a sputtered carbon layer with the separated Pt-scattering contribution of the Pt/C sample with lowest Pt loading (see Figure 5). The formation of a columnar structure even in the sputtered carbon layer is indicated by a correlation peak that is located at about the same position ($Q_{peak} \approx 0.3$ Å^{-1}) as the one of the 4w sample.

This correlation peak, however, is extremely weak and shows that the differences in the electron densities of high electron and low electron density columns are very small in this case (the main contribution to the SAXS of the carbon layer is due the porosity of carbon). Therefore, the platinum in the co-sputtered samples can only reside in the high electron density columns, since, otherwise, the correlation peak would be as weak as for the carbon layer.

The intensity model function for the columnar structure is given by

$$I(Q) = \frac{2}{\pi}\int_0^1 \left[\int_0^{\pi/2} F^2(W,L,Q_x(u,\phi),Q_y(u,\phi))d\phi\right]G^2 (\Delta C_H,\Delta C_L,D,T,Q_z(u))S(D,N_s,\sigma,Q_z(u))\,du \quad (5)$$

i.e., the intensity is averaged over all directions ($I(\boldsymbol{Q}) = I(|\boldsymbol{Q}|)$, $|\boldsymbol{Q}| = 4\pi \sin(\vartheta)/\lambda$, 2ϑ = scattering angle, λ = X-ray wavelength; for the definition of the quantities W, L, T, D, ΔC_H, ΔC_L, σ, and N_s see also Figures 4 and 6). The product $F^2 \times G^2$ is the so-called particle form factor (here, the form factor of a columnar structure element), and the function S denotes the structure factor describing interparticle interference effects (see below).

The values Q_x, Q_y, and Q_z are the components of the momentum transfer vector $\boldsymbol{Q}$ in the x, y, and z direction expressed in spherical coordinates (Q,θ,ϕ)

$$Q_x = |\boldsymbol{Q}|(1-u^2)^{1/2}\cos(\phi) \quad (6)$$

$$Q_y = |\boldsymbol{Q}|(1-u^2)^{1/2}\sin(\phi) \quad (7)$$

$$Q_z = |\boldsymbol{Q}|u \quad (8)$$

and $u = \cos(\theta)$.

A single columnar structure element, defined by a high electron density column and a low electron density column, is described by the functions

$$F(W,L,Q_x(u,\phi),Q_y(u,\phi)) = \frac{\sin\left(Q_x\frac{W}{2}\right)}{Q_x\frac{W}{2}}\frac{\sin\left(Q_y\frac{L}{2}\right)}{Q_y\frac{L}{2}}WL \quad (9)$$

and

$$G(\Delta C_H,\Delta C_L,D,T,Q_z(u)) = \Delta C_H\left(\frac{\sin\left(Q_z\frac{D}{2}\right)}{Q_z\frac{D}{2}}D - \frac{\sin\left(Q_z\frac{D-T}{2}\right)}{Q_z\frac{D-T}{2}}(D-T)\right) + \Delta C_L\frac{\sin\left(Q_z\frac{D-T}{2}\right)}{Q_z\frac{D-T}{2}}(D-T) \quad (10)$$

Since the whole sample is built up by an assembly of these elements, it is very likely that, on average, a number N_s of these columnar structure elements is more or less perfectly aligned in a certain direction (see Figure 6).

The scattering contribution of such an arrangement arising from the "intercolumn interference" has to be taken into consideration by a short-range structure factor. If it is assumed that the next-neighbor distance D of two high electron density columns obeys a Gaussian distribution, the short-range

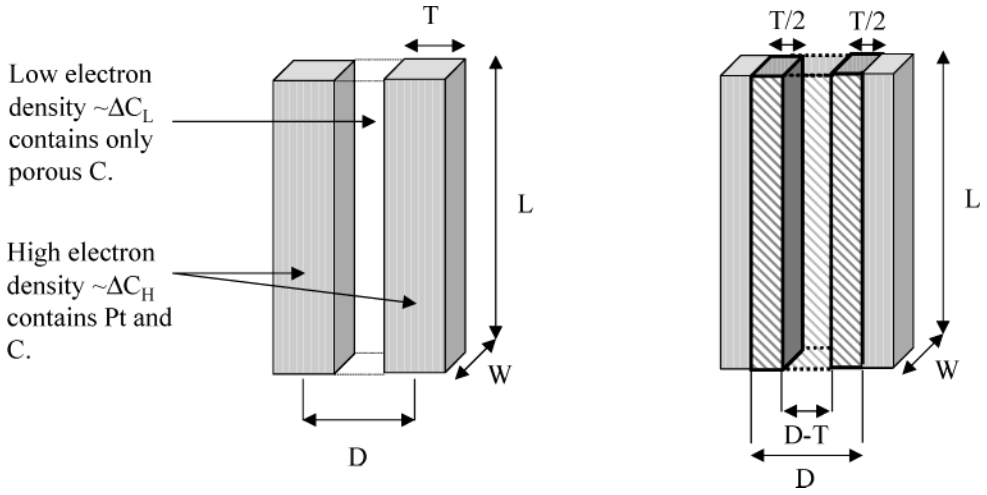

Figure 4. Left: Part of the model columnar structure consisting of two high electron density columns separated by one low electron density column for the definition of the structure parameters. Right: Same part of the columnar structure as left. The hatched area defines a single columnar structure element as used in the intensity model function (see text).

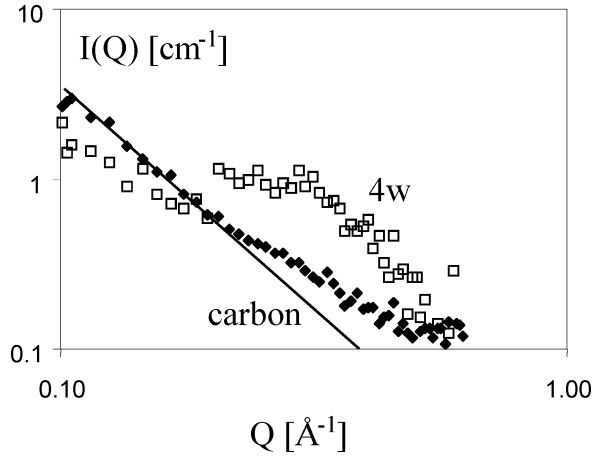

Figure 5. SAXS curve of a sputtered carbon layer compared to the separated scattering curve of the 4w sample. A very weak correlation peak located at the same position ($Q_{peak} \approx 0.3$ Å^{-1}) as the correlation peak of the 4w sample can be identified (if no correlation peak were present, the carbon scattering would follow the solid line).

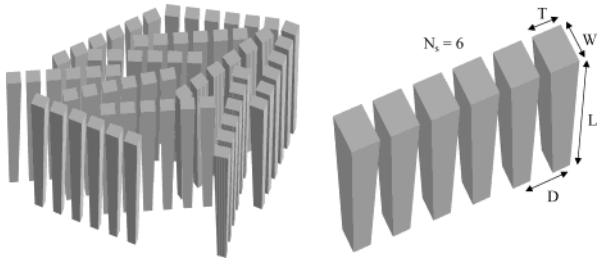

Figure 6. Example of a model columnar structure built up by several arrangements of perfectly aligned columns (left), each consisting of $N_s = 6$ single columnar structure elements (right). For the data modeling, it is furthermore assumed that these arrangements are additionally tilted against one another.

structure factor is defined as[21]

$$S(D,N_s,\sigma,Q_z(u)) = 1 + \frac{2}{N_s}\sum_{k=1}^{N_s}(N_s - k)\cos(kQ_zD)\exp\left[-\frac{k}{2}(Q_z\sigma)^2\right] \quad (11)$$

where σ represents the standard deviation of the next-neighbor distance D.

In case of separated intensities, the scattering contrast parameter is given by

$$\Delta C_{H,L}{}^2 = c_0[\Delta(nf_{H,L}(E_1))^2 - \Delta(nf_{H,L}(E_2))^2]b_0{}^2 \quad (12)$$

where $b_0 = 2.82 \times 10^{-5}$ Å is the classical electron radius.

The number density c_0 of the columnar structure elements is the ratio

$$c_0 = \frac{N_C}{V_{sa}} \quad (13)$$

where N_C is the total number of columnar structure elements in the sample and V_{sa} is the sample volume. The scattering contrast is given by the difference in the scattering-length densities of the (high/low electron density) column and the surrounding carbon matrix

$$\Delta(nf_{H,L}(E)) = \eta n_{Pt}f_{Pt}(E) + (1-\eta)n_Cf_C(E) - n_Cf_C(E) = \eta[n_{Pt}f_{Pt}(E) - n_Cf_C(E)] \quad (14)$$

The atomic form factors *f(E)* are defined by

$$f(E) = f_0 + f'(E) + if''(E) \quad (15)$$

where f_0(Pt) = 78 and f_0(C) = 6. The energy-dependent anomalous dispersion corrections $f'(E)$ and $f''(E)$[22] are depicted in Figure 7 and can be considered negligible for carbon in the vicinity of the Pt L_3 absorption edge.

The parameter η is the atomic fraction of platinum atoms relative to the carbon atoms in a column, and $n_{Pt} = 1/\Omega_{Pt}$ and $n_c = 1/\Omega_C$ are the reciprocal atomic volumes of Pt and C, respectively. Since $\eta = 0$ for the low electron density columns (the carbon matrix is defined by the low electron density columns), the scattering contrast parameter $\Delta C_L = 0$ and is therefore no longer a structure parameter for the modeling of the separated scattering intensities.

The presented scattering function is of course only valid for the case of a disordered or, at best, partly ordered, columnar structure, i.e., a structure producing a more or less isotropic scattering intensity distribution, which cannot be expected to be true for sputtered layers. In fact, the two-dimensional scattering intensity distributions of all samples are found to be anisotropic, which indicates that the columns exhibit some

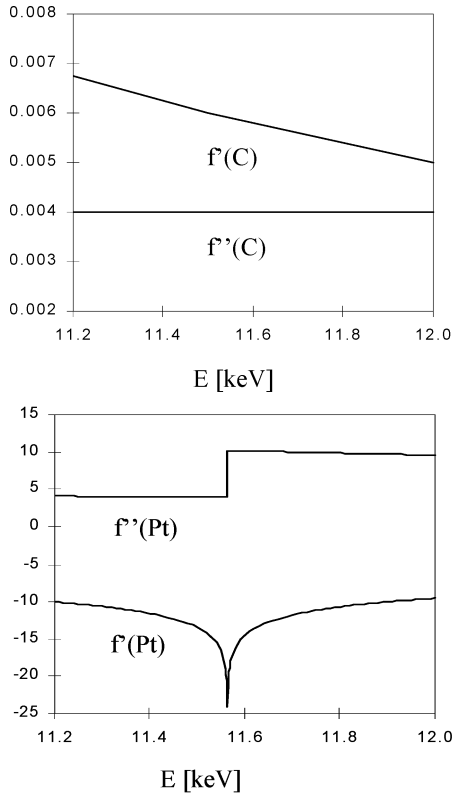

Figure 7. Anomalous dispersion corrections for carbon and platinum in the vicinity of the Pt L_3 absorption edge.

"preferred orientation". However, the anisotropy of these intensity distributions changes only slightly upon rotating the samples with respect to the incident X-ray beam (see Figure 8).

Therefore, the columns can only be partially ordered, which is already taken into account by the short-range structure factor (eq 11). Since the two-dimensional scattering patterns do not show drastic changes upon rotating the samples, i.e., no additional information on the structure, especially on the orientation of the columns, can be obtained, it is favorable to take the radial average of the two-dimensional intensity distributions (which is equivalent to an average over all orientations) and to apply an isotropic model function.

Results and Discussion

XAS. The unnormalized XAS spectra for the three Pt/C samples are shown in Figure 9. As expected, the edge jumps $\Delta\mu d$, which are proportional to the Pt content in the sample, differ clearly from one another.

The normalized absorption spectra of the three samples, compared to the one of the reference Pt foil (Figure 10), show that the platinum in the samples is in a zerovalent state, since the heights of the white lines remain unchanged. However, a systematic shift of the absorption edge energies

$$\Delta E = E_{L_3}(\text{sample}) - E_{L_3}(\text{Pt foil}) \tag{16}$$

is observed (see Table 2).

This effect may be attributed to an increase in the interaction between platinum and carbon with decreasing Pt loading. Therefore, these energy shifts indicate that either a certain amount of entirely Pt-containing regions must be present in the samples, and their concentration and/or size decreases with decreasing Pt loading, and/or that the fraction of platinum (relative to the total Pt amount) on the sample surface decreases with decreasing Pt loading.

While the first possibility is related to an decreasing Pt−Pt interaction, i.e., a decrease of metallic platinum in the sample, the second one means a simple increase in the Pt−C interaction, since Pt atoms at the surface are less surrounded by carbon atoms than in the bulk.

ASAXS. The separated scattering curves along with the fitted model intensities are depicted in Figure 11. The agreement between experimental and model intensities is excellent with respect to the data quality.

Table 3 summarizes the fit results for the dimensions of the Pt-containing (high electron density) columns W, L, and T, their average distance D, the average number of perfectly aligned columnar structure elements N_s, the scattering contrast parameter ΔC_H, and the half width at half maximum (HWHM) of the distance distribution σ. The results demonstrate that the structure parameters depend strongly on the type, in particular, the number, and the geometry of the Pt targets used for the sputtering process.

Especially the length L of the columns and the average number N_s of perfectly aligned columnar structure elements for the 4p sample differ clearly from the corresponding values of the samples 8w and 4w. The next-neighbor distance D is seemingly increasing with increasing Pt loading.

To check the quality of these results, further quantities, which are important for the characterization of electrocatalysts, can be derived from the refined structure parameters. These values can be directly compared to the results obtained from electrochemical methods, such as cyclic voltammetry (CV).

The atomic fraction η of platinum contained in a column can be estimated from the column dimensions, the scattering contrast parameter, the Pt loading, the sample thickness, and the theoretical scattering contrast of Pt and C at X-ray energies E_1 and E_2 (see eqs 12−14).

The number density c_0 of the Pt-containing columns (which is the same as that for the columnar structure elements) is given by

$$c_0 = \frac{N_C}{V_{sa}} = \frac{\left(\frac{M_{Pt}}{m_{Pt}^{col}}\right)}{A_{sa} d_{sa}} \tag{17}$$

where M_{Pt} is the total platinum mass in the sample and m_{Pt}^{col} is the platinum mass contained in a column. A_{sa} and d_{sa} are the geometric sample surface and the sample thickness, respectively.

Equation 17 can be rewritten as

$$c_0 = \frac{m(\text{Pt})}{\rho_{Pt}\eta_V V_{col} d_{sa}} \tag{18}$$

where m(Pt) is the Pt loading obtained from the absorption measurements (eq 3), ρ_{Pt} is the density of metallic platinum ($\rho_{Pt} = 21.2$ g/cm^3), η_V is the volume fraction of platinum in a column, and $V_{col} = W \times T \times L$ the volume of a column. The volume fraction η_V is related to the atomic fraction η by

$$\eta_V = \frac{1}{1 + \left(\frac{1-\eta}{\eta}\right)\frac{\Omega_C}{\Omega_{Pt}}} \tag{19}$$

where $\Omega_{Pt} = 15.1$ Å^3 and $\Omega_C = 9.06$ Å^3 are the atomic volumes of platinum and carbon. Together with the theoretical scattering

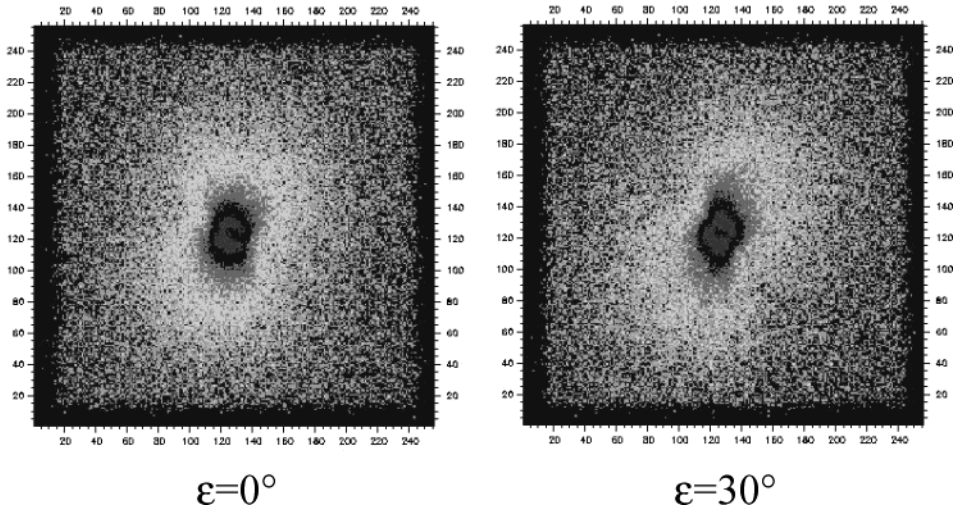

Figure 8. Two-dimensional scattering intensity distributions (raw data) of the sample 4p. Left: Surface normal of the sample and incident X-ray beam direction parallel ($\epsilon = 0°$). Right: Sample rotated by $\epsilon = 30°$ with respect to the incident beam. The main difference between the intensity distributions comes from the different transmissions the patterns have not been corrected for (the effective sample thickness increases with increasing tilt angle ϵ).

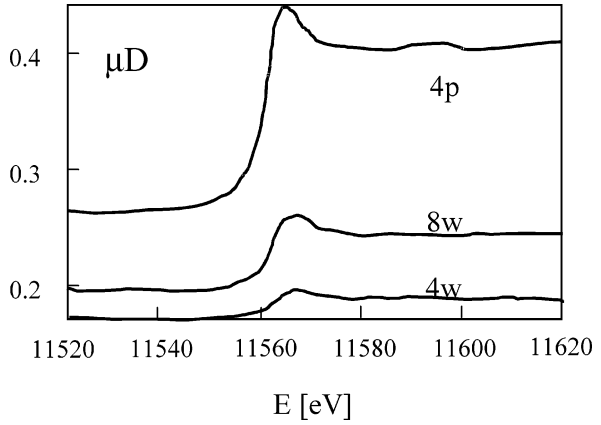

Figure 9. Unnormalized X-ray absorption spectra for Pt/C 4p, 8w, and 4w. The different edge jumps are proportional to the different Pt loadings in the samples.

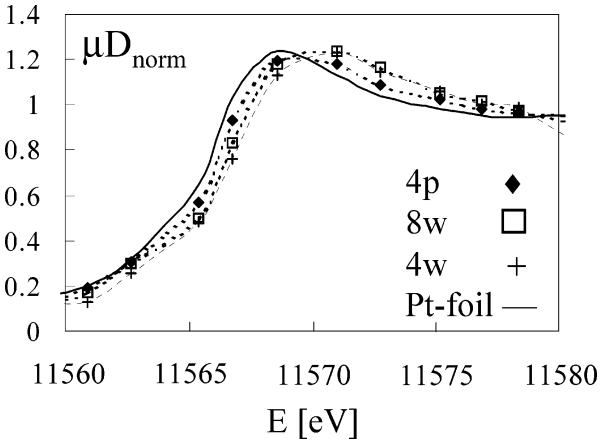

Figure 10. Normalized X-ray absorption spectra for Pt/C 4p, 8w, 4w, and the reference Pt foil. The systematic shifts of the absorption edges indicate an increasing Pt−C interaction with decreasing Pt loading.

contrast Δ_0^2 of Pt and C at the energies $E_1 = 11.437$ keV and $E_2 = 11.550$ keV

$$\Delta_0^2 = [\Delta(nf(E_1))^2 - \Delta(nf(E_2))^2]b_0^2 = 0.1586\ \text{Å}^{-3}\ \text{cm}^{-1} \quad (20)$$

TABLE 2: Pt Loading *m*(Pt), HWL (1.23 for the Reference Pt Foil), Absorption Edge Energy Shift Δ*E*, and Sample Thickness d_{sa} for the Three Pt/C Samples

sample	*m*(Pt) (mg/cm^2)	HWL	Δ*E* (eV)	d_{sa} (μm)
4p	1.288(64)	1.19(6)	0.5(3)	1.0
8w	0.468(23)	1.24(6)	1.0(3)	2.2
4w	0.207(10)	1.23(6)	1.2(3)	2.0

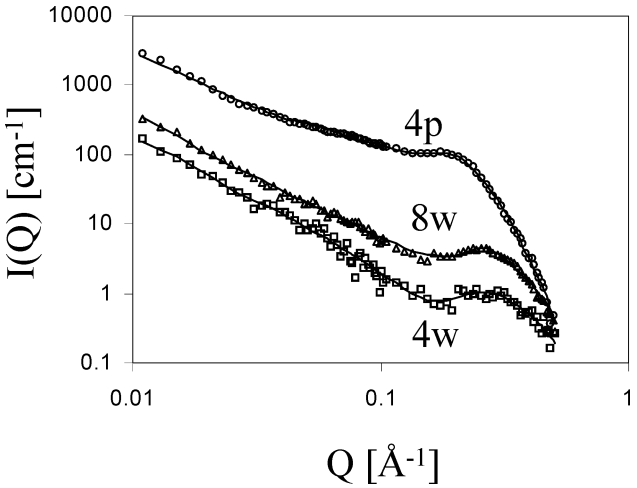

Figure 11. Separated scattering curves (symbols) and corresponding model intensities (solid lines) for the three Pt/C samples.

with $\Delta(nf(E)) = n_{Pt}f_{Pt}(E) - n_Cf_C(E)$ (i.e., $\eta = 1$), one obtains from eq 12 the relation

$$\eta^2\left(1 - \frac{\Omega_C}{\Omega_{Pt}}\right) + \eta\frac{\Omega_C}{\Omega_{Pt}} - \frac{\Delta C_H^{\ 2}}{k} = 0 \quad (21)$$

with

$$k = \frac{m(\text{Pt})\Delta_0^{\ 2}}{\rho_{Pt}V_{col}d_{sa}} \quad (22)$$

which has only one valid solution for η in the range $0 \le \eta \le 1$.[1] (It should be noted here that the same calculation was carried out for all samples with the fit results from a hard-spheres model. In this case, the η values were either negative or much larger

TABLE 3: Column Dimensions *W*, *T*, and *L*, Next-Neighbor Distance *D*, Average Number of the Columnar Structure Elements N_s, Scattering Contrast Parameter ΔC_H, and HWHM of the Distance Distribution σ for the Three Samples

sample	W (Å)	T (Å)	L (10^3Å)	D (Å)	N_s	ΔC_H (Å^{-3} cm$^{-1/2}$)	σ (Å)
4p	20.0(1)	12.8(1)	9.87(19)	28.6(2)	42(3)	$4.2(1) \times 10^{-5}$	9.6(1)
8w	12(2)	8.1(8)	2.77(32)	22(1)	14(1)	$6.7(8) \times 10^{-5}$	6.6(3)
4w	36(2)	9.6(6)	4.07(86)	16(2)	16(2)	$9.5(2) \times 10^{-6}$	7.5(6)

TABLE 4: Value $\Delta C_H^2/k$, Surface to Volume Ratio ς, Atomic Fraction η, Volume Fraction η_V, Surface Fraction η_S, Specific Active Surface A_s, and Surface Roughness A_r for the Three Pt/C Samples

sample	ΔC_H^2/k	ς (Å^{-1})	h	η_V	η_S	A_s (m^2/g)	A_r
4p	0.0463(24)	0.2565(1)	0.073(4)	0.117(6)	0.030(2)	31(2)	393(23)
8w	0.0760(230)	0.4143(280)	0.117(36)	0.182(56)	0.075(24)	81(35)	379(166)
4w	0.0162(37)	0.2644(35)	0.027(7)	0.044(10)	0.012(3)	33(11)	68(26)

than unity. Therefore, the hard-spheres model was rejected, and the columnar structure model was definitely given the preference.)

The volume fraction η_V of Pt in a column is readily obtained from eq 19. The Pt surface fraction can be approximated by

$$\eta_S = \eta_V \varsigma^* \tag{23}$$

where ς^* is the surface-to-volume ratio $\varsigma = S_{col}/V_{col}$ (formally) multiplied by 1 Å. Approximate values for the specific active surfaces of the samples are obtained from the relation

$$A_s = \frac{S(\mathrm{Pt})_{col}}{M(\mathrm{Pt})_{col}} = \frac{\eta_S S_{col}}{\rho_{Pt}\eta_V V_{col}} = \frac{\varsigma^*\varsigma}{\rho_{Pt}} \tag{24}$$

An estimate for the surface roughness, which is defined by the ratio of specific active Pt surface to specific geometric Pt surface

$$A_r = \frac{A_s}{A_g} \tag{25}$$

can also be derived from the structure parameters. Since the specific geometric Pt surface is simply given by the reciprocal value of the Pt loading m(Pt), i.e.

$$A_g = \frac{1}{m(\mathrm{Pt})} \tag{26}$$

the surface roughness is

$$A_r = A_s m(\mathrm{Pt}) \tag{27}$$

The quantities $\Delta C_H^2/k$, η, η_V, η_S, ς, A_s, and A_r are given in Table 4. The orders of magnitude for all results are seemingly correct and show that the SAXS data do not contain any severe systematic errors.

The 8w sample exhibits the best properties for an electrocatalyst material: the largest specific active surface, a surface roughness, which is comparable with the one of the 4p sample, and the best surface-to-volume ratio of the columns. Although the standard deviations of almost all these results are quite large, the values give an impression of what can be expected from the different samples under electrochemical working conditions.

For a comparison, the specific active surface and the surface roughness of all samples were also determined from the hydrogen-desorption and -adsorption peaks measured by CV (see Table 5). The experimental procedure and the estimation methods are described in details elsewhere.[8] The specific active surfaces determined by cyclic voltammetry (A_s^{CV}) as well as the surface roughness (A_r^{CV}) are systematically smaller than the values derived from the ASAXS model parameters. These

TABLE 5: Specific Active Surface A_s^{CV}, Surface Roughness A_r^{CV} Determined by CV, and Carbon Porosity *p* for the Three Pt/C Samples

sample	A_s^{CV} (m^2/g)	A_r^{CV}	$p = A_s^{CV}/A_s$ (%)
4p	15	193	48
8w	27	128	33
4w	11	23	33

differences are readily explained. For the calculation of A_s, it was neglected that the Pt-containing columns are surrounded by porous carbon (i.e., the low electron density columns). Consequently, the active surfaces estimated from the ASAXS model parameters have to be systematically larger than the values obtained from the CV experiments, since the A_s^{CV} are only determined by the active Pt sites, which have access to the electrolyte. Thus, the porosity p of the carbon material can be estimated from the ratio A_s^{CV}/A_s (see Table 5). The p values are in good agreement with the results from other studies on pure carbon thin films,[23] where porosity values between 23 and 45% were obtained. The values η_S, A_s, and A_r show that the fraction of platinum on the sample surface (relative to the total Pt amount) does not increase systematically with increasing Pt loading. Therefore, the systematic shifts of the absorption edge energies observed in the XAS spectra can be explained by an increase of only Pt-containing regions, i.e., inhomogeneities in the spatial distribution of Pt, with increasing Pt loading.

The assumed formation of platinum metal clusters is also supported by the characterization of these samples using X-ray photo electron spectroscopy (XPS). The full width at half maximum for the Pt 4f signal measured by XPS decreased with increasing Pt loading, indicating the formation of larger Pt particles.[8] The Pt inhomogeneities should also be reflected by the model parameters. The formation of metal clusters is leading to a decrease of the specific active Pt surface. The A_s values derived from the model structure parameters and the Pt loading of the samples (see Table 4) actually show such a tendency. The specific active surface for both the 8w and 4w samples is larger than the one of the 4p sample. While the relative change in the absorption edge energy shifts between 4p and 8w are quite large ($[\Delta E(8w) - \Delta E(4p)]/\Delta E(8w) = 100\%$, see Table 2), the relative change between 8w and 4w is about 17%, i.e., the metal-cluster fractions in 8w and 4w are not very different, so that the specific active surface should be only dependent on the Pt loading of the samples, which is easily confirmed by the good agreement of the ratios $A_s(8w)/A_s(4w) = 2.4$ and $m(\mathrm{Pt},8w)/m(\mathrm{Pt},4w) = 2.3$. These considerations show that the proposed model describes the nanostructures of the co-sputtered Pt/C layers sufficiently well and confirms that both model and model parameters are physically reasonable.

Conclusions

The results demonstrate that the technique of ASAXS is a suitable method for the characterization of co-sputtered Pt/C layers. In combination with X-ray absorption measurements and CV experiments, a full quantitative analysis is possible. The X-ray absorption spectra disclose that the Pt−Pt interaction is increasing with increasing Pt loading, which indicates the formation of Pt clusters. However, the relative amount of Pt contained in such metal clusters, compared to the total Pt content, must be very small since the attempt to fit the separated scattering intensities with a hard-spheres model led to unphysical results. The nanostructures of the Pt/C layers are found to be well described by a columnar structure model. Especially the values for the specific active surface and surface roughness derived from the model parameters are (qualitatively) in excellent agreement with the results obtained from CV and prove that the proposed model is physically reasonable. Therefore, the presented results can be considered as a basis for further systematic studies, which have to be performed in order to unravel the relationships between structural properties, electrochemical properties, and sample preparation conditions.

References and Notes

(1) Reddington, E.; Sapienza, A.; Gurau, B.; Viswanathan, R.; Sarangapani, S.; Smotkin, E. S.; Mallouk, T. E. *Science* **1998**, *280*, 1735.

(2) Ticianelli, E. A.; Derouin, C. R.; Srinivasan, S. *J. Electroanal. Chem.* **1988**, *251*, 275.

(3) Enea, O.; McEvoy, A. J. *Ultramicroscopy* **1992**, *42*−*44*, 572.

(4) Cong, P. J.; Doolen, R. D.; Fan, Q.; Giaquinta, D. M.; Guan, S. H.; McFarland, E. W.; Poojary, D. M.; Self, K.; Turner, H. W.; Weinberg, W. H. *Angew. Chem. Int. Ed.* **1999**, *38*, 484.

(5) Witham, C. K.; Chun, W.; Valdez, T. I.; Narayanan, S. R. *Electrochem. Solid-State Lett.* **2000**, *3*, 497.

(6) Hayre, R. O.; Lee, S. J.; Cha, S. W.; Prinz, F. B. *J. Power Sources* **2002**, *109*, 483.

(7) Hirano, S.; Kim, J.; Srinivasan, S. *Electrochim. Acta* **1997**, *42*, 1587.

(8) Hajbolouri, F.; Scherer, G. G.; Vad, T.; Abolhassani-Dadras, S.; Schnyder, B.; Horisberger, M.; Wokaun, A. In preparation.

(9) Hajbolouri, F.; Scherer, G. G.; Vad, T.; Horisberger, M.; Schnyder, B.; Wokaun, A. *PSI Scientific Report* **2002**, *Vol. V*, 83.

(10) Haubold, H.-G.; Gebhardt, R.; Buth, G.; Goerigk, G. In *Resonant Anomalous X-ray Scattering, Theory and Applications*, Materlik, G., Sparks, C. J., Fischer, K., Eds.; Elsevier Science: Oxford, 1994; p 295.

(11) Haubold, H.-G.; Wang, X. H. *Nucl. Instrum. Methods B* **1995**, *97*, 50.

(12) Haubold, H.-G.; Gruenhagen, K.; Wagner, M.; Jungbluth, H.; Heer, H.; Pfeil, A.; Rongen, H.; Brandenburg, G.; Moeller, R.; Matzerath, J.; Hiller, P.; Halling, H. *Rev. Sci. Instrum.* **1989**, *60*, 1943.

(13) Haubold, H.-G.; Wang, X. H.; Jungbluth, H.; Goerigk, G.; Schilling, W. *J. Mol. Struct.* **1996**, *383*, 283.

(14) Vad, T.; Haubold, H.-G.; Waldöfner, N.; Bönnemann, H. *J. Appl. Crystallogr.* **2002**, *35*, 459.

(15) Brown, M.; Peierls, R. E.; Stern, A. *Phys. Rev. B* **1977**, *15*, 738.

(16) Mattheiss, L. F.; Dietz, R. E. *Phys. Rev. B* **1980**, *22*, 1663.

(17) Röhler, J. *J. Magn. Magn. Mater.* **1995**, *47/48*, 175.

(18) Vrij, A. *J. Chem. Phys.* **1979**, *71*, 3267.

(19) Movchan, B. A.; Demchishin, A. V. *Fiz. Metal. Metalloved* **1969**, *28*, 653.

(20) Thornton, J. A. *J. Vac. Sci. Technol.* **1974**, *11*, 666.

(21) Kratky, O.; Porod, G. *J. Colloid Sci.* **1949**, *4*, 35.

(22) Cromer, D. T.; Liberman, D. A. *Acta Crystallogr. A* **1981**, *37*, 267.

(23) Braun, A.; Bärtsch, M.; Schnyder, B.; Kötz, R.; Haas, O.; Haubold, H.-G.; Goerigk, G. *J. Non-Cryst. Sol.* **1999**, *260*, 1.